Electronic Supplementary Material (ESI) for Nanoscale.

Reversible light-dependent molecular switches on Ag/AgCl nanostructures

W. Song, C. J. Querebillo, R. Götz, S. Katz, U. Kuhlmann, U. Gernert, I. M. Weidinger, and P. Hildebrandt

Table of Contents

1. **Experimental details**
2. **Substrate characterization**
3. **SER spectra of 4-NTP on Ag/AgCl and Ag supports**
4. **SER spectra of 4-ATP on Ag/AgCl and Ag supports**
5. **References**

1. Experimental Procedures

Chemicals and Materials. Silver foil (0.025 mm thick, annealed, 99.95% (metal basis)) was purchased from Alfa Aesar. Iron(III) chloride ($FeCl_3$, reagent grade, 97%) was purchased from Sigma-Aldrich. p-Aminothiophenol (4-ATP) was purchased from Wako Pure Chemical Industry. 4-Nitrothiophenol (4-NTP) (98%) was purchased from abcr GmbH. Na_2CO_3 and ethanol were purchased from Sigma-Aldrich and used without further purification. All reagents were used as received without further purification. Milli-Q water was used for the whole synthesis.

Preparation of AgCl particles deposited on the surface of silver foil (Ag/AgCl substrate). Ag/AgCl substrates were produced by immersing a silver foil into a $FeCl_3$ aqueous solution with a concentration of 10^{-2} M for 1 min at T= 298 K, followed by thorough rinsing with distilled water (50 mL) for three times, then drying under a stream of nitrogen gas.

SERS-active Ag/AgCl substrates for the SER spectroscopic investigations. The Ag/AgCl substrates (ca. 5 mm × 5 mm) was immersed into 200 µL of 4-NTP or 4-APT ethanolic solution (10^{-3} M) for 24 h, subsequently washed with ethanol to remove excess of 4-NPT/4-ATP and dried with nitrogen gas. The sample was then inserted into an aqueous solution, buffered to the desired pH. During the "laser on" or "light" period, the laser beam was focused to the same spot of the sample with a laser power of 1 mW (unless indicated otherwise). Accumulation time for the spectra was usually 1 s. The "laser-off" or "dark" period referred to ambient light conditions.

Instrumentation. SEM and EDX measurements were carried out using a JEOL JSM-6700F field emission scanning electron microscope (FE-SEM) operated at 3.0 kV.
SER spectra were obtained with a HR800 Raman Spectrometer (Horiba), the 514.5 nm radiation from the Ar^+ ion laser (Coherent) was used as excitation source. Further details of the Raman spectroscopic set-up are given elsewhere [1].
XRD pattern was acquired on a SmartLab 3 Intelligent XRD system (Rigaku) with CuKα radiation.
XPS measurements were carried out using a Thermo ESCALAB 250 photoelectron spectrometer with Al Ka X-ray radiation.

Calculations. All calculated Raman spectra were computed by density functional theory (DFT) within the program package Gaussian 09 [2]. The functional BP86 [3,4] and the basis set 6-31g* were used. The initial structure for the optimization was constructed by Gaussview. To include the effect of the solvent (water), the Polarizable Continuum Model (PCM) was applied in all calculations [5].

2. Substrate characterization

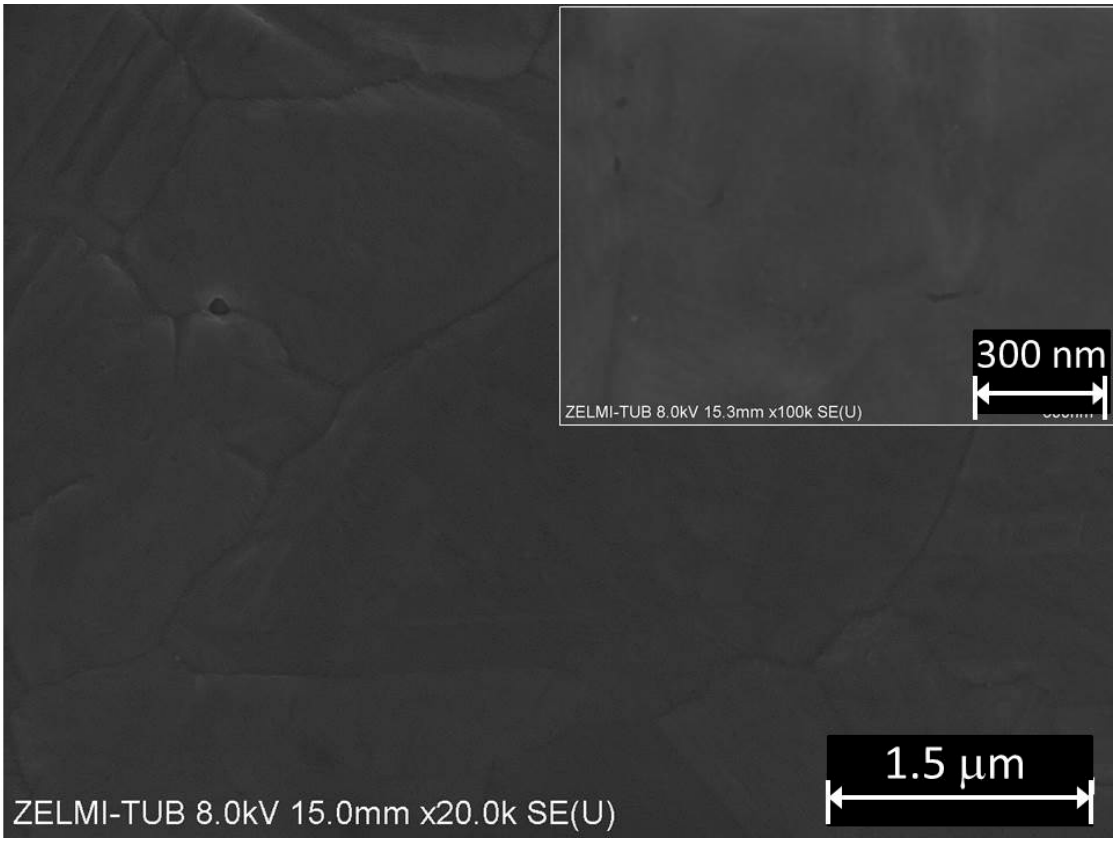

Figure S1. SEM image of the unetched Ag foil. The inset shows a higher magnification of the Ag foil.

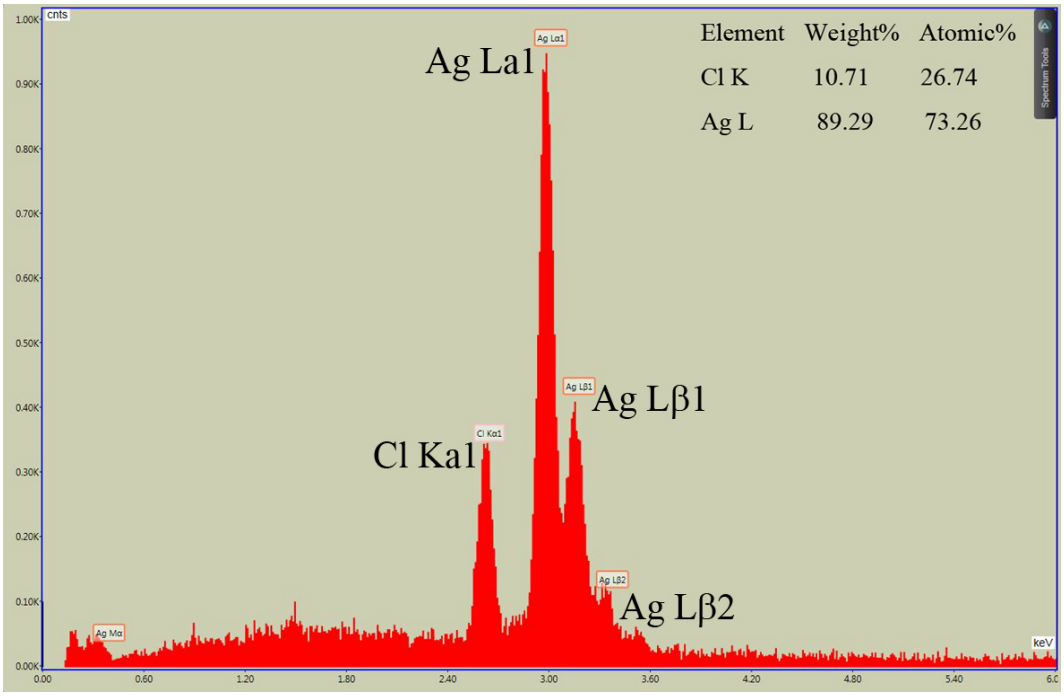

Figure S2. EDX spectrum of the as-prepared Ag/AgCl substrate.

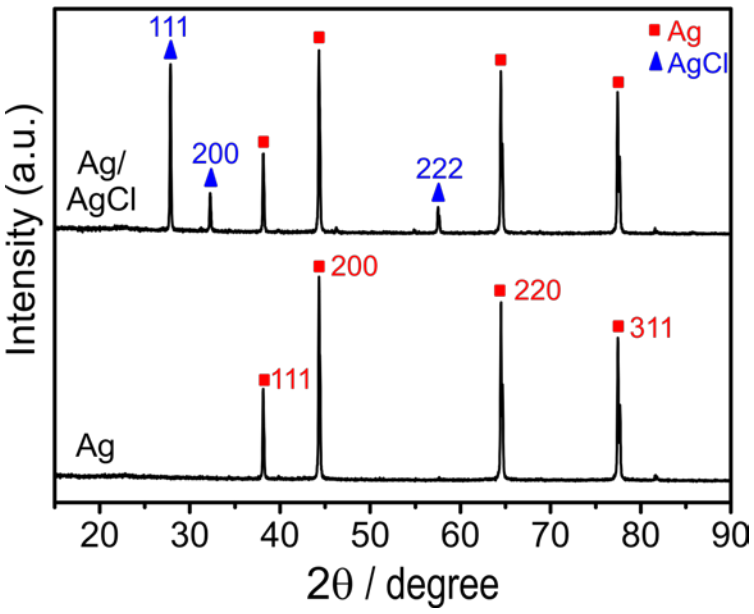

Figure S3. XRD patterns of the Ag foil (bottom) and the Ag/AgCl substrate (top).

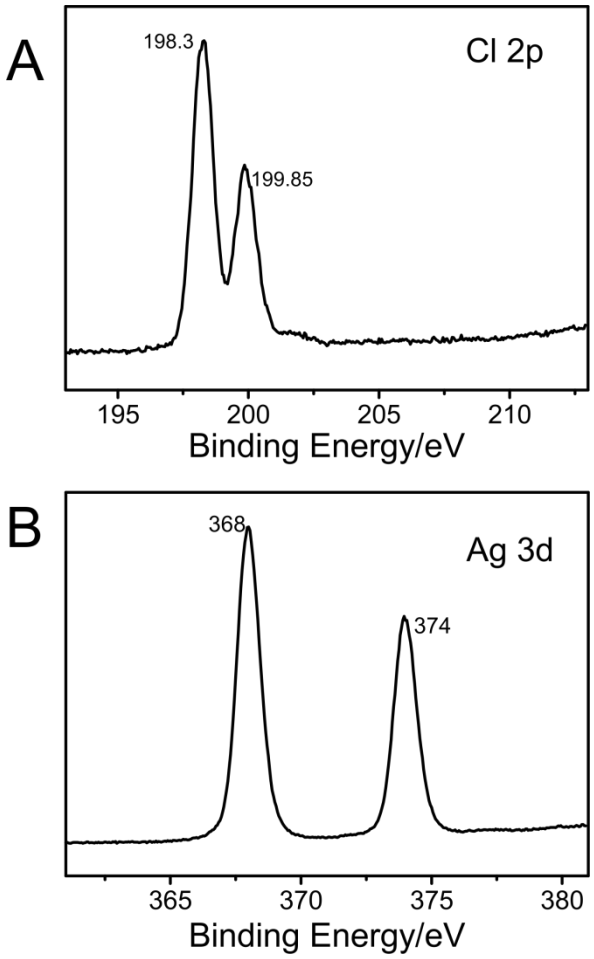

Figure S4. XPS measurements of the Ag/AgCl substrate.

3. SER spectra of 4-NPT

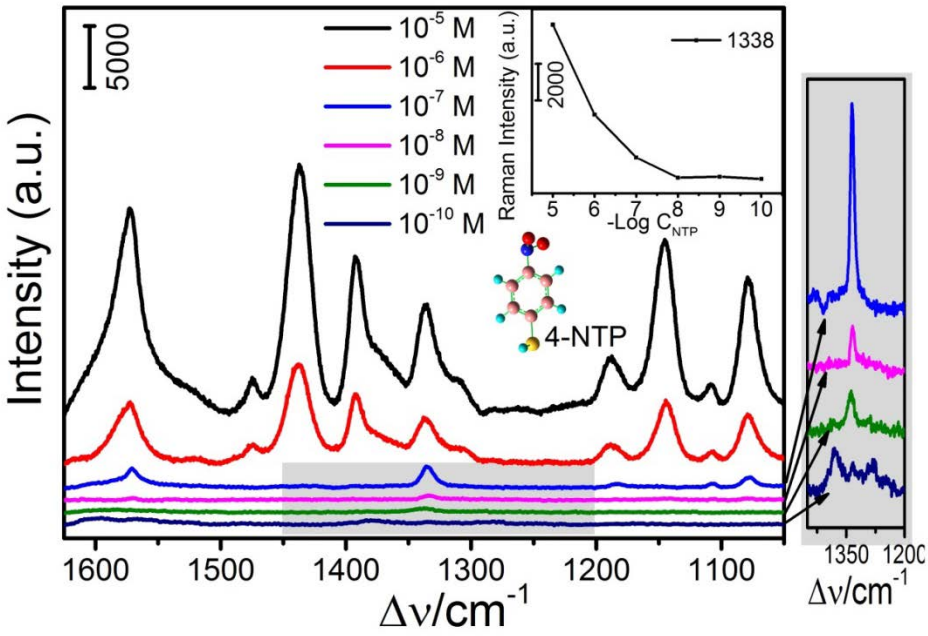

Figure S5. SER spectra of 4-NTP adsorbed on Ag/AgCl at different 4-NPT concentrations in solution. The accumulation time was 10 s and the laser power was 0.1 mW.

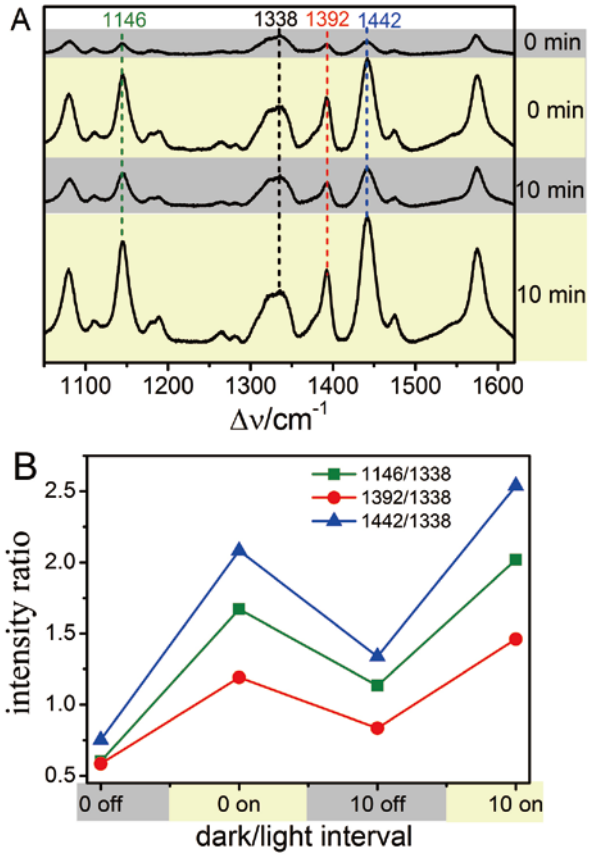

Figure S6. A, Light-dependent switching behaviour of 4-NTP adsorbed on Ag/AgCl at pH = 10.0. Spectra were measured for 1 s (2.4 mW) at the end of the dark and light periods (10 minutes each) as indicated in the figure. **B**, Plot of the intensity ratios of the bands at 1146, 1392 and 1442 cm^{-1} (DMAB) with respect to the 4-NTP band at 1338 cm^{-1} as a function of the dark and light intervals.

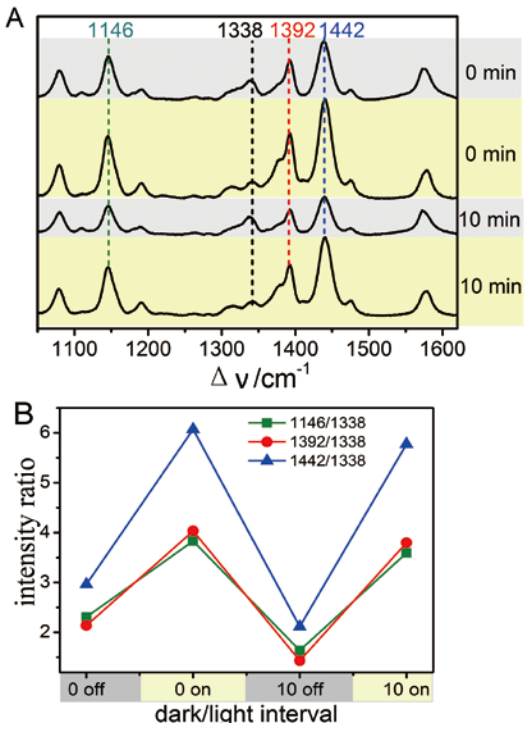

Figure S7. A, Light-dependent switching of 4-NTP adsorbed on Ag/AgCl at pH = 4.0. Spectra were measured for 1 s (1 mW) at the end of the dark and light periods (10 minutes each) as indicated in the figure. **B**, Plot of the intensity ratios of the bands at 1146, 1392 and 1442 cm^{-1} (DMAB) with respect to the 4-NTP band at 1338 cm^{-1} as a function of the dark and light intervals.

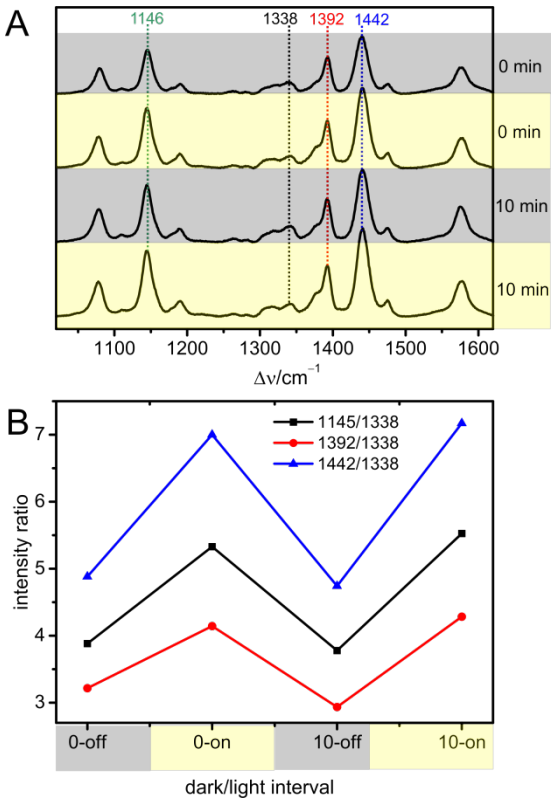

Figure S8. A, Light-dependent switching of 4-NTP adsorbed on Ag/AgCl at pH = 7.0. Spectra were measured for 1 s (1 mW) at the end of the dark and light periods (10 minutes each) as indicated in the figure. **B**, Plot of the intensity ratios of the bands at 1146, 1392 and 1442 cm^{-1} (DMAB) with respect to the 4-NTP band at 1338 cm^{-1} as a function of the dark and light intervals.

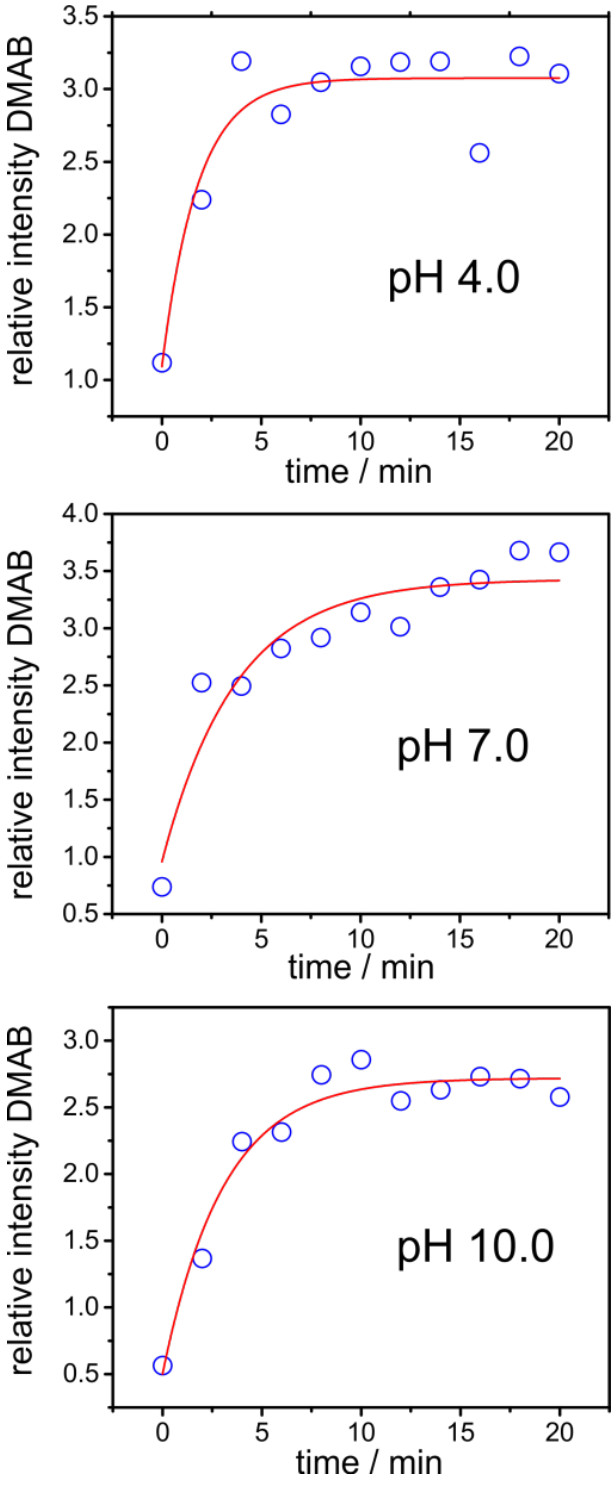

Figure S9. Plot of the intensity ratio of the 1442/1338 cm^{-1} bands determined for 4-NTP/DMAB on Ag/AgCl at different pH under continuous laser irradiation. The red solid lines represent fits of exponential functions to the data.

The fits afforded apparent rate constants k_{light} for the processes under laser irradiation of $9.2 \cdot 10^{-3}$ s^{-1} at pH 4.0, $4.5 \cdot 10^{-3}$ s^{-1} at pH 7.0, and $5.5 \cdot 10^{-3}$ s^{-1} at pH 10.0. The corresponding rate constants k_{dark} for the processes in the dark interval were estimates from the intensity drops after switching off the laser (see for example, Figures S7B, S8B, and 3B), affording $1.5 \cdot 10^{-3}$ s^{-1} at pH 4.0, $0.5 \cdot 10^{-3}$ s^{-1} at pH 7.0, and $4.0 \cdot 10^{-3}$ s^{-1} at pH 10.0.

The apparent rate constants k_{light} describe the temporal evolution of the quasi-photostationary equilibrium of the reactions (A = 4-NTP; D = DMAB)

(1) $A + A \overset{h\nu\,\Delta\;\Delta}{\rightarrow\rightarrow\rightarrow} \ldots . D$

(2) $D \overset{h\nu\,\Delta\;\Delta}{\rightarrow\rightarrow\rightarrow} \ldots . A + A$

The reaction sequences of (1) and (2) are initiated by a primary photoprocess (hν) followed by thermal reaction steps (Δ). One may now approximate the kinetic description of theses sequences by a single effective rate constant k_{dim} for (1) and k_{mon} for (2). Both k_{dim} and k_{mon} include the photochemical rate constant of the primary event and the thermal rate constants of the consecutive reaction steps. This is in line with (a) the pH dependence of k_{light} which should only refer to thermal processes and (b) the power-dependence of the switching behavior (photostationary equilibrium; cf. Figure 5 and Figure S6) which reflects the involvement of the photochemical reaction step. One may therefore approximate k_{dim} and k_{mon} by a product of the photochemical (pH-independent) and thermal (pH-dependent) contribution according to

(3) $k_{dim} = k_{dim,h\nu} \cdot k_{dim,\Delta}$

(4) $k_{mon} = k_{mon,h\nu} \cdot k_{mon,\Delta}$

At sufficiently long irradiation times, the quasi-photostationary equilibrium

(5) $K = \frac{[D]}{[A]^2} = \frac{k_{dim}}{k_{mon}} = \frac{k_{dim,h\nu} \cdot k_{dim,\Delta}}{k_{mon,h\nu} \cdot k_{mon,\Delta}}$

is reached. In the dark period, the thermal reaction sequence of DMAB dissociation continues such that it appears to be justified to assume $k_{dark} \cong k_{mon,\Delta}$. Thus one obtains from eq. 5

(6) $K \cdot k_{dark} = \frac{k_{dim,h\nu} \cdot k_{dim,\Delta}}{k_{mon,h\nu}}$

The quantity *K* can be expressed by the intensity ratio *R* of 4-NTP and DMAB bands according to

(7) $K = R \cdot \frac{f_{DMAB}}{f_{4-NTP}^2} = R \cdot F$

where $f_{4\text{-NTP}}$ and f_{DMAB} are proportionality factors that relate the relative concentrations to the reciprocal SER cross sections of the specific bands. These factors are not known but can be considered to be pH independent and may therefore be summarized in a mode-specific pH-independent factor *F*. Using the NO_2 stretching of the unperturbed 4-NTP (γ-band at ca. 1340 cm^{-1}) and the 1392 cm^{-1} band of DMAB (Figure 8), the following parameters can now be determined:

pH	***R***	$\boldsymbol{k_{dark}/s^{-1}}$	$\boldsymbol{\frac{k_{dim,h\nu} \cdot k_{dim,\Delta}}{k_{mon,h\nu} \cdot F}/s^{-1}}$	$\boldsymbol{k_{light}/s^{-1}}$
4.0	7.7	$1.5 \cdot 10^{-3}$	$11.6 \cdot 10^{-3}$	$9.2 \cdot 10^{-3}$
7.0	5.5	$0.5 \cdot 10^{-3}$	$2.8 \cdot 10^{-3}$	$4.5 \cdot 10^{-3}$
10.0	1.0	$4.0 \cdot 10^{-3}$	$4.0 \cdot 10^{-3}$	$5.5 \cdot 10^{-3}$

The data show that the pH dependence of the term $\frac{k_{dim,h\nu} \cdot k_{dim,\Delta}}{k_{mon,h\nu} \cdot F}$ and thus $k_{dim,\Delta}$ follows the same tendency as k_{light}. Thus, we conclude dimerization is strongly favored at low pH whereas the reverse reaction (k_{dark}) is accelerated at high pH.

4. SER spectra of 4-ATP

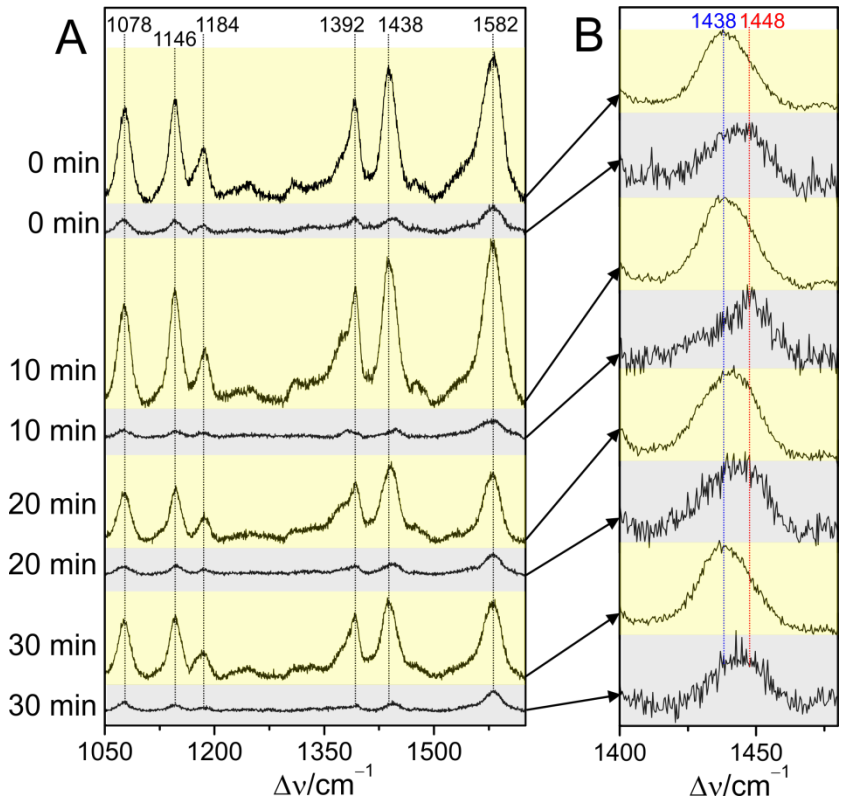

Fig. S10. A, B. Light-dependent switching behaviour of 4-ATP adsorbed on Ag/AgCl at pH = 4.0. The spectra were measured consecutively (accumulation time 1 s) in steps of 1 minute. Dark and light (laser irradiation on) intervals (in minutes) are highlighted in grey and yellow, respectively. **B** shows an enlarged view of the spectral region between 1400 and 1480 cm^{-1}. Here the relative intensities were re-scaled (compared to **A**) to highlight the spectral changes of the 1438/1448 cm^{-1} doublet.

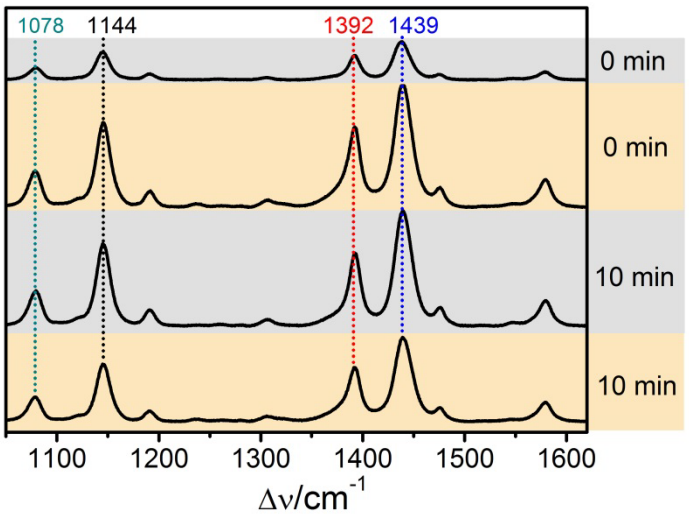

Figure S11. SER spectra of 4-ATP adsorbed on Ag/AgCl at pH = 10.0, measured for 1 s (1 mW) at the end of the dark and light periods as indicated in the figure. The spectra reveal no indication for light/dark- or time-dependent cis-trans isomerisation as observed for pH 4.0.

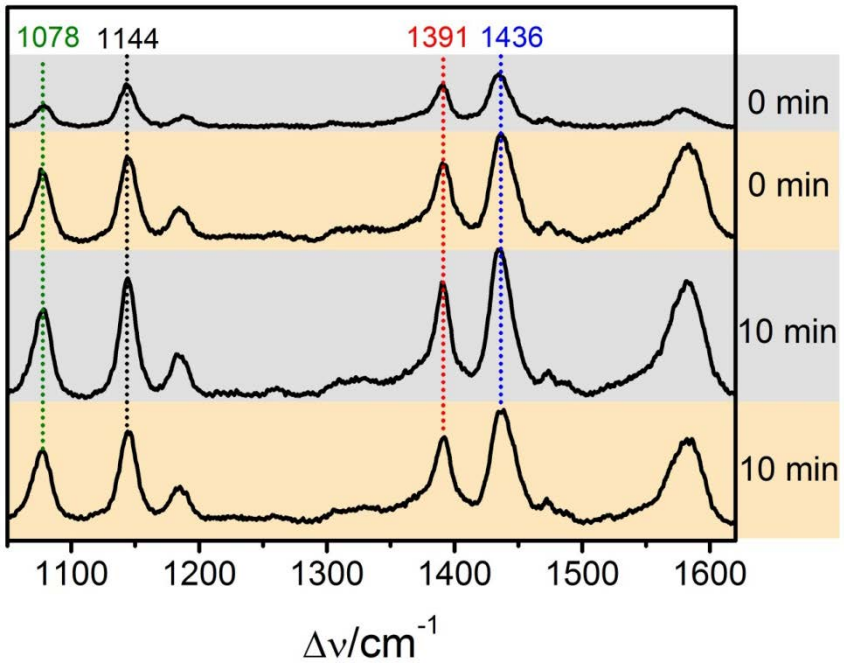

Figure S12. SER spectra of 4-ATP adsorbed on rough Ag surface at pH = 4.0, measured for 1 s (1 mW) at the end of the dark and light periods as indicated in the figure. The spectra reveal no indication for light/dark- or time-dependent cis-trans isomerisation as observed for Ag/AgCl substrates at pH 4.0.

5. References

[1] E. Siebert, Y. Rippers, S. Frielingsdorf, J. Fritsch, A. Schmidt, J. Kalms, S. Katz, O. Lenz, P. Scheerer, L. Paasche, V. Pelmenschikov, U. Kuhlmann, M. A. Mroginski, I. Zebger, P. Hildebrandt, *J. Phys. Chem. B* **2015**, *119*, 13785−13796.

[2] M. J. Frisch, G. W. Trucks, H. B. Schlegel, G. E. Scuseria, M. A. Robb, J. R. Cheeseman, G. Scalmani, V. Barone, B. Mennucci, G. A. Petersson, H. Nakatsuji, M. Caricato, X. Li, H. P. Hratchian, A. F. Izmaylov, J. Bloino, G. Zheng, J. L. Sonnenberg, M. Hada, M. Ehara, K. Toyota, R. Fukuda, J. Hasegawa, M. Ishida, T. Nakajima, Y. Honda, O. Kitao, H. Nakai, T. Vreven, J. A. Montgomery, Jr., J. E. Peralta, F. Ogliaro, M. Bearpark, J. J. Heyd, E. Brothers, K. N. Kudin, V. N. Staroverov, R. Kobayashi, J. Normand, K. Raghavachari, A. Rendell, J. C. Burant, S. S. Iyengar, J. Tomasi, M. Cossi, N. Rega, J. M. Millam, M. Klene, J. E. Knox, J. B. Cross, V. Bakken, C. Adamo, J. Jaramillo, R. Gomperts, R. E. Stratmann, O. Yazyev, A. J. Austin, R. Cammi, C. Pomelli, J. W. Ochterski, R. L. Martin, K. Morokuma, V. G. Zakrzewski, G. A. Voth, P. Salvador, J. J. Dannenberg, S. Dapprich, A. D. Daniels, Ö. Farkas, J. B. Foresman, J. V. Ortiz, J. Cioslowski, and D. J. Fox, Gaussian, Inc., Wallingford CT, 2009.

[3] J. P. Perdew, Phys. Rev. B: Condens. Matter Mater. Phys., 1986, 33, 8822.

[4] A. D. Becke, Phys. Rev. A: At., Mol., Opt. Phys., 1988, 38, 3098.

[5] J. Tomasi, B. Mennucci, and R. Cammi, “Quantum mechanical continuum solvation models,” Chem. Rev., 105 (2005) 2999-3093.

[6] F. J. Vidal-Iglesias, J. Solla-Gullón, J. M. Orts, A. Rodes, J. M. Pérez, *J. Phys. Chem. C* 2015, 119, 12312-12324.